Available online at www.sciencedirect.com
SCIENCE DIRECT®
PERGAMON
International Journal of Heat and Mass Transfer 46 (2003) 4561–4571
International Journal of HEAT and MASS TRANSFER
www.elsevier.com/locate/ijhmt

Mechanism of gas absorption enhancement in a slurry droplet containing reactive, sparingly soluble microparticles

M.K. Akbar, J. Yan, S.M. Ghiaasiaan *

George W. Woodruff School of Mechanical Engineering, Georgia Institute of Technology, Atlanta, GA 30332-0405, USA

Received 21 February 2003; received in revised form 10 June 2003

Abstract

The absorption of a gaseous species by a slurry droplet containing reactive and sparingly soluble microparticles is numerically simulated. The problem studied is relevant to spray flue gas desulfurization systems and the objective of this study was to elucidate the effect of the reactive solid particles on the parameters that determine the mass transfer processes. Spherical droplets with internal circulation similar to Hill's vortex flow were considered. Quasi-steady conservation equations representing the absorbed and dissolved reactant species and equations representing the dissolution of particles were numerically solved using the droplet internal circulation streamline as a coordinate. Second-order and instantaneous chemical reactions were both addressed. The results show that the reactant microparticles enhance the absorption rate by increasing the gradient of the absorbed species beneath the droplet surface. The relative effect of solid particles depends strongly on the droplet internal circulation and diminishes as stronger recirculation occurs.

Keywords: Flue gas desulfurization; Slurry droplet; Absorption; Chemical reaction; Numerical; Droplet recirculation; Reaction layer

1. Introduction

Flue gas desulfurization (FGD) is often achieved using limestone slurry droplets in a spray or packed tower [1]. In the former, water spray droplets saturated with dissolved limestone and containing microparticles of limestone, are sprayed into the flue gas. The presence of the sparingly soluble limestone particles is believed to enhance the absorption rate of sulfur dioxide. Most of the published studies dealing with the basic FGD processes have addressed gas absorption in bubbling slurry reactors [2–9]. Furthermore, virtually all relevant models are based on the Higbie's penetration theory [1,2,10] or Whitman's film theory [11]. In these models, due to the low diffusivity of the absorbed species and the fast chemical reaction, the chemical reaction is believed to take place within a thin liquid film beneath the gas–liquid interface (the reaction layer). The enhancement of the absorption process by the reactant microparticles, it has been argued [2,12], can be achieved when these particles are much smaller in diameter than the thickness of the aforementioned reaction film and occurs because the dissolution of the particles distorts the concentration profiles of the reacting species.

Published studies dealing with the spray FGD process are relatively limited [10,11,13]. The chemistry of the FGD in a droplet without internal circulation has been studied in [13]. Mehra [10], also modeling a droplet without internal circulation using Higbie's penetration theory, showed that the reactant particles in the reaction film can undergo significant shrinkage and neglecting this shrinkage can lead to over prediction of the absorption rate. Recognizing the significance of droplet internal circulation, Muginstein et al. [11] recently modeled a slurry droplet based on Whitman's film theory, assuming a uniform reaction film thickness and a constant tangential liquid velocity equal to the droplet surface velocity at its equator.

* Corresponding author. Tel.: +1-404-894-3746; fax: +1-404-894-8496.
E-mail address: seyed.ghiaasiaan@me.gatech.edu (S.M. Ghiaasiaan).

0017-9310/$ - see front matter © 2003 Elsevier Ltd. All rights reserved.
doi:10.1016/S0017-9310(03)00296-5

Nomenclature

A	Hill's vortex strength ($m^{-1}\,s^{-1}$)
A	absorbed species
A_p	total solid particle surface area concentration (m^{-1})
B	solid (reactant) species
C	reaction product species; concentration ($k\,mol/m^3$)
C_D	drag coefficient
D	slurry droplet diameter (m)
D	diffusivity (m^2/s)
d_p	solid particle diameter (m)
h	dimensionless coordinate scale factor
i	mesh index for ξ coordinate
j	mesh index for ζ coordinate
k_2	second-order reaction constant ($m^3/k\,mol\,s$)
k_{2A}	second-order reaction constant for species A ($m^3/kg\,s$)
k_{2B}	second-order reaction constant for species B ($m^3/kg\,s$)
K_s	mass transfer coefficient between solid particles and liquid (m/s)
M	molecular mass number (kg/k mol)
N_P	particle number density in the slurry (m^{-3})
Pe	Peclet number
R	droplet radius (m)
r	radial coordinate (m)
Re_G	droplet Reynolds number
s	distance along particle path (m)
Sh	Sherwood number
t	time (s)
U	dimensionless liquid velocity
u	liquid velocity (m/s)
u_e	surface velocity at droplet equator
$u_{e,m}$	maximum surface velocity at droplet equator
u_r	reference velocity ($=\frac{2}{3}u_e$)
u_∞	droplet's terminal velocity (m/s)
w	volume fraction of solid particles
X	normalized mass fraction
x	mass fraction
Y	mole fraction
z	coefficient in the chemical reaction

Greek symbols

β	dimensionless parameter defined in Eq. (22)
Δ	parameter defined in Eq. (29)
δ	thickness of the diffusion layer (m)
Γ	dimensionless parameter defined in Eq. (21)
η	dimensionless radial coordinate
λ	thickness of the reaction layer (m)
μ	dynamic viscosity (kg/ms)
ν	kinematic viscosity (m^2/s)
θ	tangential coordinator in polar spherical coordinates (R)
ρ	density (kg/m^3)
Ω_A, Ω_B	dimensionless parameters defined in Eqs. (19) and (20)
ξ	parameter defined in Eq. (24)
ψ_L	stokes stream function (m^3/s)
ζ	variable defined in Eq. (25)

Subscripts

A	absorbed species
B	reactive species
i	gas–liquid interphase
L	liquid
l	droplet lower hemisphere
P	particle
s	saturated with respect to dissolved species B
u	droplet upper hemisphere

Superscript

*	dimensionless

In this paper the gas absorption process in a spherical, non-oscillating slurry droplet that undergoes internal circulation is numerically simulated. The objective of the reported study was to elucidate the details of the mass transfer processes and examine the mechanism by which the solid reactant particles may influence these processes.

2. Physical system and assumptions

Although the chemistry of FGD is complicated [13,14], it is often simplified by an instantaneous or second-order chemical reaction between the absorbed gas A and the dissolved, sparingly soluble reactive species B according to [6,10,11]:

$$A + zB \rightarrow \text{Products} \tag{1}$$

Fig. 1 is a schematic of a modeled droplet. Slurry droplets are typically about 1 mm in diameter and contain limestone particles typically a few μm in diameter. For such droplets undergoing free fall in flue gas, $Re_G \approx 300$–400. Droplets with sufficiently strong surface tension remain approximately spherical and non-oscillating within the latter range [15]. For spherical droplets with creep flow ($Re_G < 1$) the droplet internal circulation follows the well-known Hadamart–Rybczinski solution [16,17]. At higher Re_G values, as long as the droplet re-

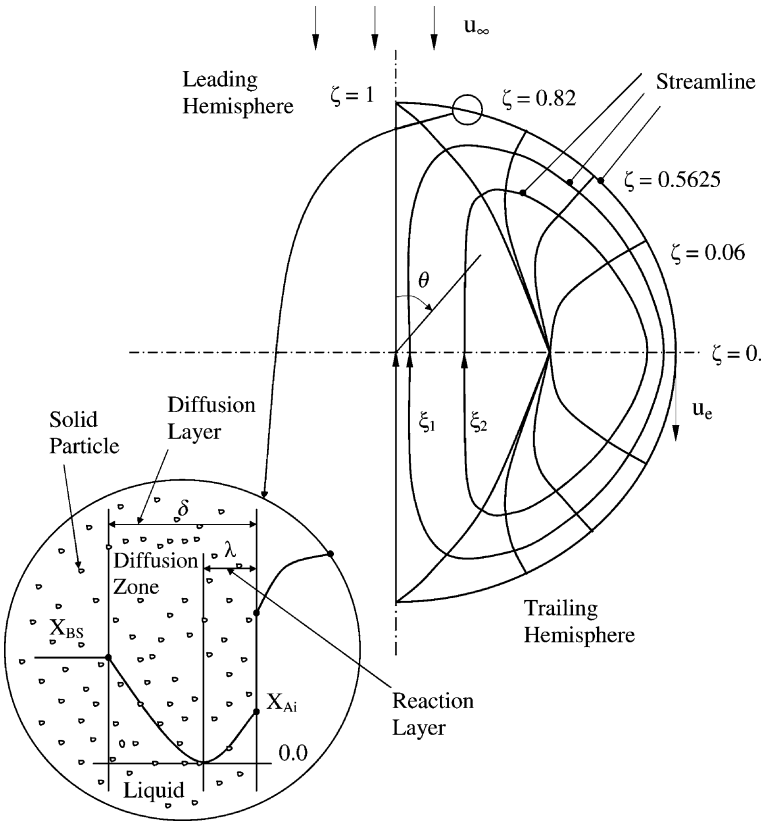

Fig. 1. Schematic of the modeled system.

mains spherical and the internal circulation motion is assumed inviscid [18], the following equation for Stokes' stream function approximately applies to the droplet's inviscid core [18,19]:

$$\psi_{\mathrm{L}} = \frac{1}{2} A r^2 (R^2 - r^2) \sin^2 \theta \tag{2}$$

Eq. (2) is identical to the Hadamard–Rybczynski, if A is found from:

$$A = \frac{u_\infty}{2R^2(\mu_{\mathrm{L}}/\mu_{\mathrm{G}} + 1)} \tag{3}$$

For $Re_{\mathrm{G}} \gg 1$ and in the absence of surface active contaminants, however [19]:

$$A = 1.5 u_\infty R^{-2} \tag{4}$$

The droplet internal circulation configuration is qualitatively depicted in Fig. 1. The species concentration profiles depicted represent infinitely fast reaction kinetics and define the reaction and diffusion layers [2,12]. Absorption of species A takes place at the surface of the droplet, while chemical reaction between A and B occurs in the liquid phase. Species A and B evidently have to diffuse in opposite directions, and for an infinitely fast reaction the two species can not coexist anywhere. A thin reaction layer and a wider diffusion layer thus form, starting near the leading pole of the droplet and develop along the droplet surface. The closed streamlines move through the droplet internal wake after passing the vicinity of the droplet rear pole. For the diffusion of a single species without chemical reaction, based on dimensional analysis, an estimate of the diameter of the droplet internal wake is $RPe^{-1/4}$ [20]. Mixing can be expected in the droplet interior wake and fresh liquid would emerge at the vicinity of the droplet leading pole. The droplet internal recirculation can thus lead to a quasi-steady state process whereby the liquid in the droplets near-surface streamlines undergo a cycle during each circulation period. For an infinitely fast reactions complete depletion of dissolved species B should occur in the reaction layer. The small solid particles of species B are expected to enhance the absorption process by their slow dissolution, if they are small compared with the thickness of the reaction layer, λ.

The following assumptions are made in accordance with the above discussion:

1. The slurry droplet is spherical and non-oscillating; with an internal circulation similar to Hill's vortex flow.
2. Each solid particle in the droplet slurry moves along the streamline of and with the same velocity as, its surrounding liquid.
3. The gas-side mass transfer resistance associated with the transfer of species A to the droplet is negligible in comparison with the liquid-side resistance.
4. The droplet interior is saturated with respect to dissolved species B.
5. The chemical reaction between A and B is either infinitely fast, or is second order.
6. The mass transfer process is quasi-steady.
7. The solid particles are spherical and are made of pure species B.

Justification for assumption 1 has been provided in the aforementioned discussion. Assumption 2 is appropriate in view of the small size of the particles and the typically short droplet recirculation period that renders Brownian dispersion of particles negligible. Assumptions 3–5 are also all reasonable. The sixth assumption is also reasonable since the droplet recirculation period is of the order D/u_e and is therefore much shorter than the order of magnitude of the characteristic time associated with a significant change in the slurry droplet's make-up. The last assumption is a simplifying idealization.

3. Mathematical model

The mass conservation equation for species A and B, both sparingly can be written as:

$$\rho_L \vec{u} \cdot \nabla x_A = \rho_L \nabla .(D_A \nabla x_A) - k_{2A} \rho_L^2 x_A x_B \tag{5}$$

$$\rho_L \vec{u} \cdot \nabla x_B = \rho_L \nabla \cdot (D_B x_B) - k_{2B} \rho_L^2 x_A x_B + N_p \pi d_p^2 \rho_L K_s (x_{BS} - x_B) \tag{6}$$

where, due to the low solubility of either species in the liquid:

$$k_{2A} = k_2 / M_B \tag{7}$$

$$k_{2B} = k_2 / M_A \tag{8}$$

The microparticles undergo slow dissolution according to:

$$\rho_P \vec{u} \cdot \nabla d_P = -2\rho_L K_s (x_{BS} - x_B) \tag{9}$$

The boundary conditions are as follows. At the droplet surfaces $(\nabla x_B) \cdot \vec{N} = 0$ and $x_A = x_{A,i}$; where $x_{A,i}$ represents the solubility of species A in the liquid corresponding to the system temperature and the partial pressure of A in the surrounding gas and $\vec{N}$ represents a unit normal vector; $x_A = 0$ and $x_B = x_{BS}$ at the leading pole on the droplet surface; and $x_B = x_{BS}$ deep inside the droplet. Due to the very small size of particles, molecular diffusion is the primary mechanism for mass transfer between the solid particles and the liquid, therefore:

$$Sh_p = K_s d_p / D_B = 2 \tag{10}$$

The above equations can be normalized assuming that D_A and D_B are constants, using $u_r = \frac{2}{3} u_e$ as reference velocity, d_{p_o} as the reference particle diameter and R as the reference length scale everywhere else, to get:

$$\vec{U} \cdot \nabla^* X_A = 2 Pe_A^{-1} \nabla^{*^2} X_A - \Omega_A X_A X_B \tag{11}$$

$$\vec{U} \cdot \nabla^* X_B = 2 Pe_B^{-1} \nabla^{*^2} X_B - \Omega_B X_A X_B + \Gamma (1 - X_B) \tag{12}$$

$$\vec{U} \cdot \nabla^* d_p^* = -\beta (1 - X_B) \tag{13}$$

where

$$X_A = x_A / x_{Ai} \tag{14}$$

$$X_B = x_B / x_{BS} \tag{15}$$

$$d_p^* = d_p / d_{p_o} \tag{16}$$

$$Pe_A = 2 u_r R / D_A \tag{17}$$

$$Pe_B = 2 u_r R / D_B \tag{18}$$

$$\Omega_A = \frac{\rho_L R k_2}{u_r M_B} x_{BS} \tag{19}$$

$$\Omega_B = \frac{\rho_L R k_2}{u_r M_A} x_{Ai} \tag{20}$$

$$\Gamma = \pi N_p R d_p^2 K_s / u_r \tag{21}$$

$$\beta = 2 \rho_L R K_s x_{BS} / (\rho_p u_r d_{p_o}) \tag{22}$$

Surface-active contaminants can significantly reduce the droplet internal recirculation [15,17,21]. In the absence of surface-active contaminants, however, the droplet surface velocity at its equator is related to the droplet's terminal velocity according to (see Eq. (4)):

$$u_e = u_{e,m} = \tfrac{2}{3} u_\infty \tag{23}$$

The aforementioned dimensionless equations are now cast in the (ξ, ζ, ϕ) coordinates, where $\xi = \text{const}$ represents a closed internal circulation streamline and [22,23]:

$$\xi = 4\eta^2 (1 - \eta^2) \sin^2 \theta \tag{24}$$

$$\zeta = \frac{\eta^4 \cos^4 \theta}{2\eta^2 - 1} \tag{25}$$

$$h_\xi = 8\eta \sin \theta \sqrt{\Delta} \tag{26}$$

$$h_\zeta = \frac{(2\eta^2 - 1)^2}{4\eta^3 \cos^3 \theta \sqrt{\Delta}} \tag{27}$$

$$h_\phi = \eta \sin\theta \tag{28}$$

$$\Delta = (1-\eta^2)^2 \cos^2\theta + (2\eta^2-1)^2 \sin^2\theta \tag{29}$$

$$\eta = r/R \tag{30}$$

It can also be shown that [22]:

$$(1-\eta^2)^2(2\eta^2-1)\zeta - \left[\eta^2(1-\eta^2) - \frac{1}{4}\xi\right]^2 = 0 \tag{31}$$

In writing the species conservation equations, symmetry with respect to ϕ is assumed. The species conservation equations can then be represented as:

$$U\frac{(\xi,\zeta)}{h_\zeta}\frac{\partial X_A}{\partial \zeta} = \left(\frac{1}{h_\xi h_\zeta h_\phi}\right)\frac{2}{Pe_A}\left[\frac{\partial}{\partial \xi}\left(\frac{h_\zeta h_\phi}{h_\xi}\frac{\partial X_A}{\partial \xi}\right) + \frac{\partial}{\partial \zeta}\left(\frac{h_\xi h_\phi}{h_\zeta}\frac{\partial X_A}{\partial \zeta}\right)\right] - \Omega_A X_A X_B \tag{32}$$

$$U\frac{(\xi,\zeta)}{h_\zeta}\frac{\partial X_B}{\partial \zeta} = \left(\frac{1}{h_\xi h_\zeta h_\phi}\right)\frac{2}{Pe_B}\left[\frac{\partial}{\partial \xi}\left(\frac{h_\zeta h_\phi}{h_\xi}\frac{\partial X_B}{\partial \xi}\right) + \frac{\partial}{\partial \zeta}\left(\frac{h_\xi h_\phi}{h_\zeta}\frac{\partial X_B}{\partial \zeta}\right)\right] - \Omega_B X_A X_B + \Gamma(1-X_B) \tag{33}$$

The particle mass conservation equation, furthermore, gives:

$$\frac{U(\xi,\zeta)}{h_\zeta}\frac{\mathrm{d}d_p^*}{\mathrm{d}\zeta} = -\beta(1-X_B) \tag{34}$$

The dimensionless fluid velocity resulting from Eqs. (2) and (4) is [15]:

$$U(\eta,\theta) = \frac{3}{2}\{(1-\eta^2)^2\cos^2\theta + (1-2\eta^2)^2\sin^2\theta\}^{\frac{1}{2}} \tag{35}$$

The boundary conditions for Eqs. (32)–(34) are as follows: At $\zeta = 1$, in the leading hemisphere (see Fig. 1): $\mathrm{d}p^* = 1$, $X_A = 0$ and $X_B = 1$. At $\xi = 0$, representing the droplet surface: $X_A = 1$, $\partial X_B/\partial \xi = 0$. Deep inside the droplet, represented by $1 \leqslant \xi \leqslant 0$: $X_A = 0$ and $X_B = 1$. Finally, at $\zeta = 1$ in the trailing hemisphere, $\partial X_A/\partial \zeta = \partial X_B/\partial \zeta = 0$ is assumed.

4. Numerical solution method

Eqs. (32)–(34) were numerically solved, using the finite-difference technique, in the pseudo-rectangle defined by $0 \leqslant \xi \leqslant \xi_{max}$, $0 \leqslant \zeta \leqslant \zeta_{o,u}$ and $0 \leqslant \zeta \leqslant \zeta_{o,l}$, where $\zeta_{o,u} = |\zeta_{o,l}| = 0.95$ were assumed. The latter assumed values correspond to $1.6° \leqslant \theta \leqslant 178.4°$ on the droplet surface. Based on scoping calculations, $\xi_{max} = 0.5$ was used and parametric calculations all indicated that the latter value for ξ_{max} was quite adequate. The computational domain is depicted in Fig. 2. A non-uniform mesh size distribution was used and based on extensive convergence tests, the number of mesh points were 1000 for ξ and 1600 for ζ in all parametric calculations. Calculations showed that increasing the mesh numbers beyond the aforementioned values caused negligibly small changes in the results. An outline of the nodalization

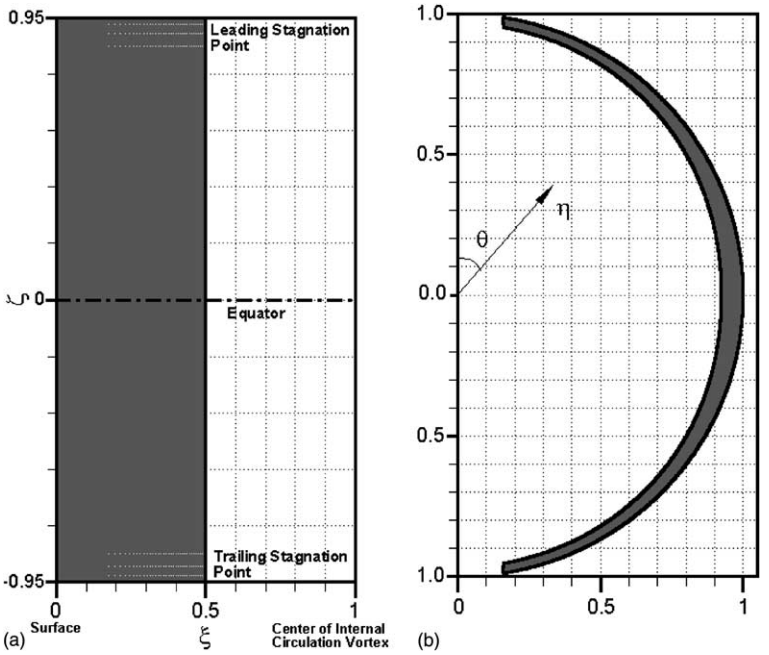

Fig. 2. Computation domain: (a) transformed (in ξ, ζ) shape and (b) actual shape.

scheme and the numerical solution method is provided in the Appendix A.

5. Results and discussion

For parametric calculations the standard thermophysical and transport property values for CO_2–$Ca(OH)_2$, proposed and used by Mehra [10], were applied. Accordingly, for all (default) parametric calculations $C_{Ai} = 3 \times 10^{-2}$ k mol/m^3 and $C_{BS} = 9 \times 10^{-2}$ k mol/m^3 were assumed, leading to $X_{Ai} = 1.32 \times 10^{-3}$ and $X_{BS} = 4.44 \times 10^{-3}$. Other default parameters were: $D_A = D_B = 2 \times 10^{-9}$ m^2/s; $k_2 = 1 \times 10^8$ m^3/k mol s; and $\rho_p = 1.5 \times 10^3$ kg/m^3. For the liquid, water properties at 300 K were used. The terminal velocity of the spray droplet was calculated using the correlation of Lapple [15] for drag coefficient:

$$u_\infty = \left[\frac{4D(\rho_L - \rho_G)g}{3C_D\rho_G}\right]^{\frac{1}{2}} \tag{36}$$

$$C_D = \frac{24}{Re_G}[1 + 0.125Re_G^{0.72}] \tag{37}$$

where $Re_G = u_\infty D/\nu_G$ and ν_G is the kinematic viscosity of standard atmospheric air.

For a contaminant-free droplet unimpeded internal circulation would lead to Eq. (23). Significantly reduced droplet internal circulation may be expected in FGD systems, however, and will be considered in the forthcoming parametric calculations. The effect of the solid reactant particles, furthermore, will be addressed by parametrically varying w, the initial volume fraction of particles in the slurry droplet.

Concentration profiles for a droplet 1 mm in diameter, in free fall in gas and with internal circulation ten times slower than that for a surface active-contaminant free droplet ($u_e = \frac{1}{10}u_{e,m}$), are displayed in Fig. 3, where a second-order chemical reaction has been assumed. The depicted concentration profiles in represent the radial variations of the normalized mass fractions of species A and B at azimuthal angles $\theta = 45°$, 90°, 135° and 178.4°,

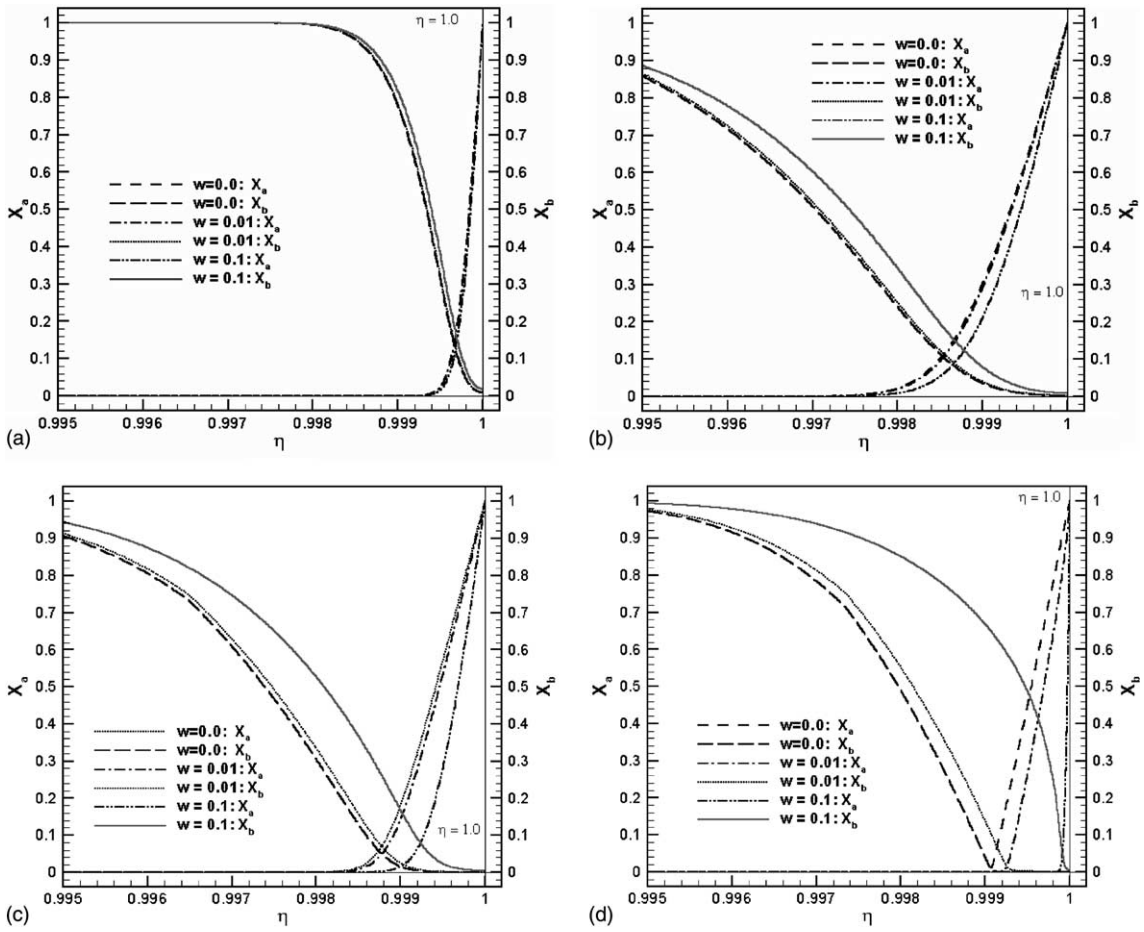

Fig. 3. Effect of solid particles on concentration profiles for the second-order reaction, with droplet recirculation 10 times slower than that for an unimpeded recirculation: (a) 45°, (b) 90°, (c) 135° and (d) 178.4°.

respectively (see Fig. 1). These figures also show the effect of the volume fraction of the solid particles (w) on the concentration profiles. The solid particles were assumed to be 2 μm in diameter initially and uniformly distributed in the liquid. The development of the reaction layer (defined as the zone where $X_A > 0$), and the diffusion layer (defined as the zone where $X_B < 1$) along the droplet surface and the influence of the reactant solid particles on them, can be readily noticed. Due to the finite reaction rate, the two reacting species coexist virtually in the entire reaction layer thickness. The development of the reaction and diffusion layers is complicated due to the recirculation velocity. In the droplet leading hemisphere, down to the droplet equator, these layers both grow in thickness as a result of the diffusion process and more importantly due to the favorable circulation velocity effect which tends to expand the streamlines (Fig. 3(a and b)). An opposite trend is observed in the droplet southern hemisphere, however (Fig. 3(c and d)). These opposing circulation velocity effects are due to the fact that the lateral distance between specific circulation streamline pairs increases as the equator is approached and the opposite occurs when the fluid moves away from the equator in the trailing hemisphere.

The influence of particles is easily discernible in Fig. 3(a–d). The presence of solid particles evidently does not cause a significant qualitative effect in the shapes of the concentration profiles. The particles, however, tend to reduce the thickness of both reaction and diffusion layers, leading to a steeper concentration gradient species A, and hence an enhanced absorption rate. This effect of the particles on the species A concentration gradient grows in strength along the streamlines and is particularly significant near the droplet trailing pole.

Concentration profiles and the effect of the solid particle volume fraction on them, are depicted in Fig. 4(a–d) for an instantaneous chemical reaction ($k_2 = \infty$).

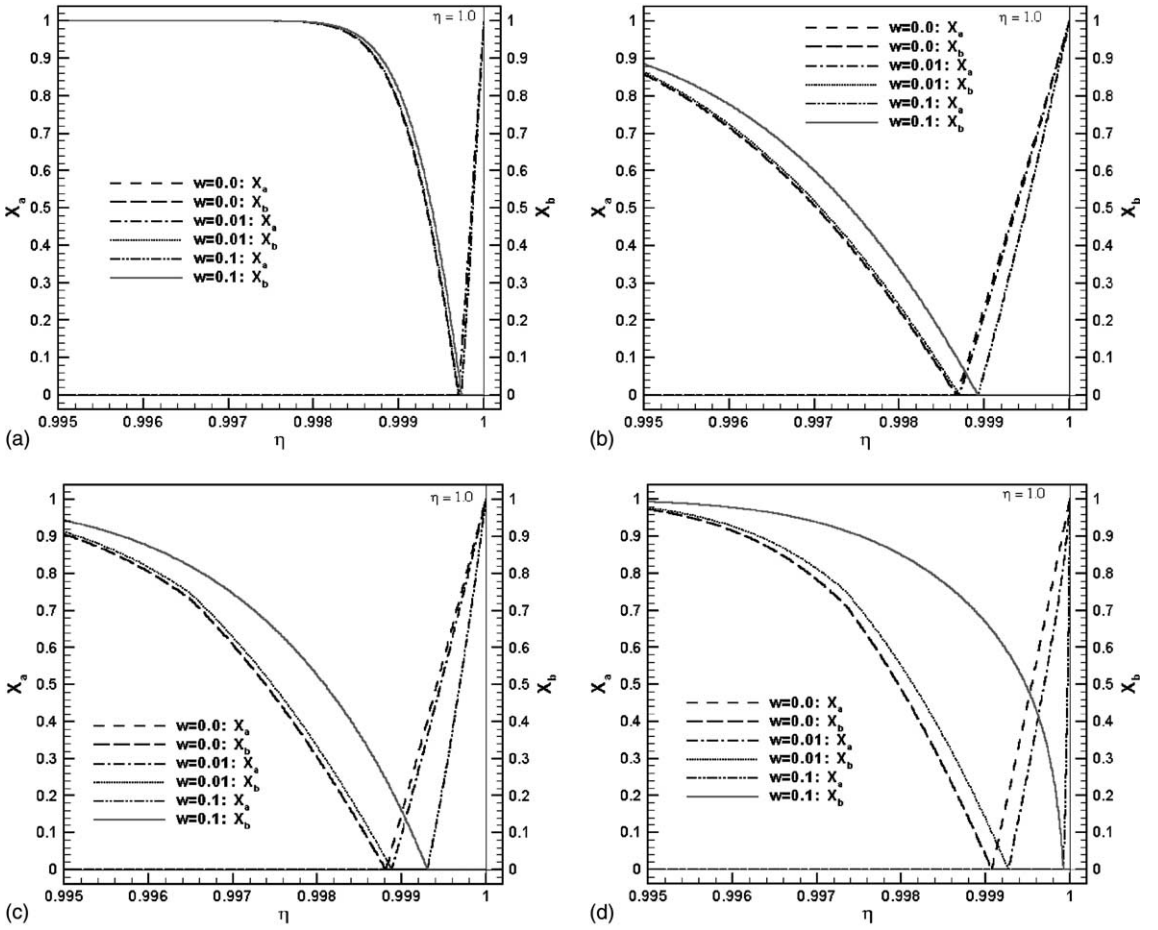

Fig. 4. Effect of solid particles on concentration profiles for an instantaneous reaction, with droplet recirculation 10 times slower than that for an unimpeded recirculation: (a) 45°, (b) 90°, (c) 135° and (d) 178.4°.

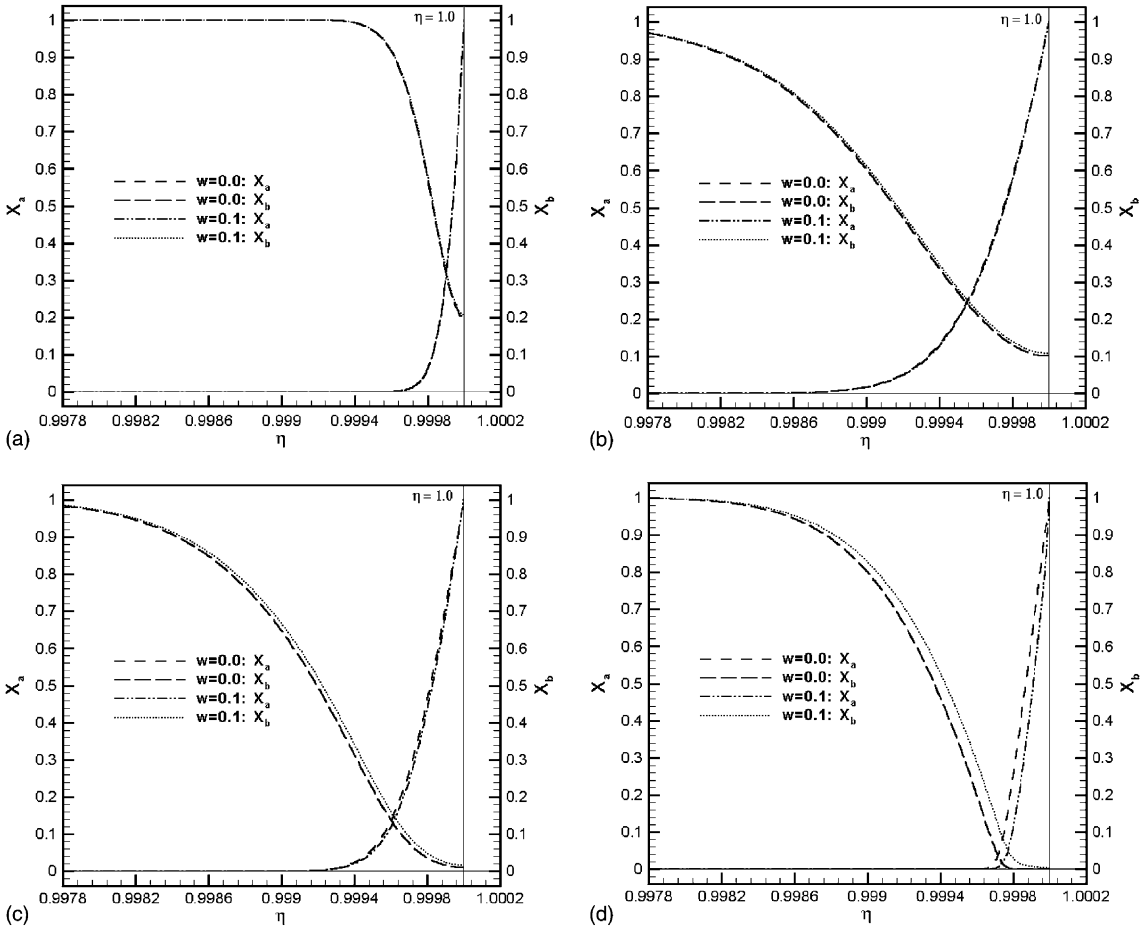

Fig. 5. Effect of solid particles on concentration profiles for the second-order reaction, with unimpeded droplet recirculation: (a) 45 °, (b) 90°, (c) 135° and (d) 178.4°.

The instantaneous chemical reaction renders the profiles qualitatively different than those depicted in Fig. 3(a–d). With $k_2 \to \infty$, the concentrations of both species vanish at the edge of the reaction layer, as expected; the reaction layer is everywhere significantly thinner than the reaction layer with finite k_2; and hence significantly higher concentration gradients of species A occur everywhere. The influence of the solid particles on the concentration profiles and the reaction layer is similar to those described for Fig. 3(a–d), however, and higher volume fractions of the solid particle lead to thinner reaction layer and higher species A concentration beneath the droplet surface.

The enhancing influence of particles on the absorption rate depends on the duration of the exposure time of the liquid surface to the gas. A shorter exposure duration would lead to smaller enhancement effect of the solid particles and for extremely short exposure times the effect of solid particles will be negligible [24]. Smaller effects of solid particles on the concentration profiles should thus be expected as stronger droplet internal circulations are considered. Figs. 5 and 6 are similar to Figs. 3 and 4, respectively, with the difference that the droplet internal circulation in the simulations represented by Figs. 5 and 6 is assumed to be unimpeded, whereby $u_e = u_{e,m} = \frac{3}{2}u_\infty$. Curves representing $w = 0.01$ are not displayed in the latter figures since they are virtually indistinguishable from the curves representing $w = 0.1$. The concentration profiles are of course everywhere steeper in these figures than their counterparts representing lower droplet recirculation, evidently as a result of shorter exposure times in the former. The effect of the reactant solid particles on the concentration profiles and the reaction layer thickness, although qualitatively similar to those discussed earlier (i.e., thinner reaction layers and steeper transferred species concentration profiles due to solid particles), are small, indicating that relatively insignificant absorption enhancement can be achieved by adding solid particles to droplets with fast, unimpeded internal circulation.

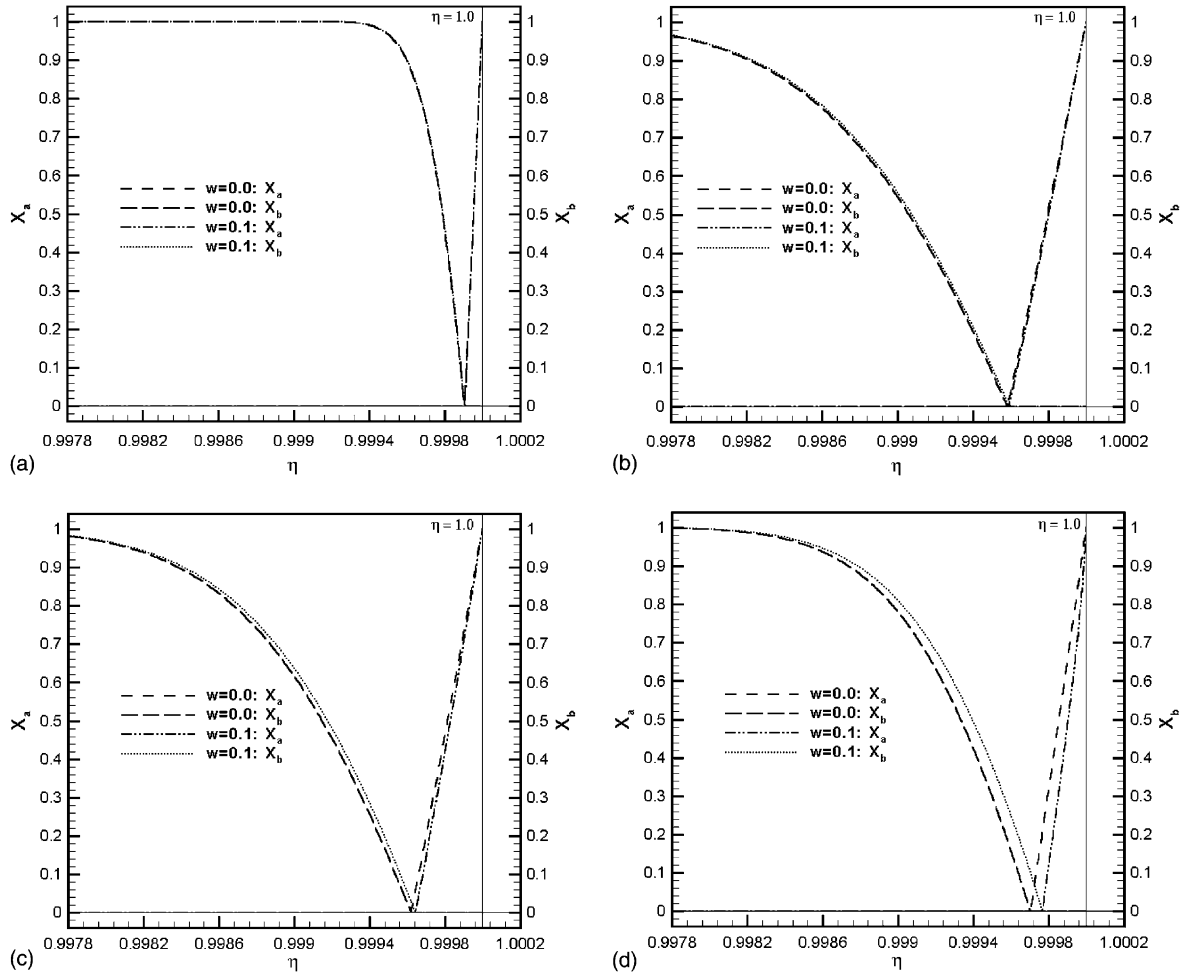

Fig. 6. Effect of solid particles on concentration profiles for an instantaneous reaction with unimpeded droplet recirculation: (a) 45°, (b) 90°, (c) 135° and (d) 178.4°.

The dissolution of particles evidently leads to their shrinkage. Mehra [10] has showed that, for a droplet with no internal circulation, the solid particle size change is important. Typical model-predicted particle size variations are depicted in Fig. 7, where the variations of d_p/d_{p_o} along the streamlines are shown, with d_{p_o} representing the particle average diameter as it emerges to the droplet surface near its leading pole. These results indicate trends consistent with the concentration profiles discussed earlier. The variations in particle diameter in a single recirculation period are evidently very small, however.

Using the numerical models described in this paper, extensive parametric calculations have been performed that examine the effect of various parameters, as well as particle size variations, on droplet absorption rates. The quasi-steady droplet mass transfer and reaction models have also been utilized for the development of a transient model that accounts for the effect of time variation of average solid particle diameter on the droplet absorption rates. These parametric results and the transient model are described in [25].

6. Concluding remarks

A numerical study aimed at the elucidation of the effect of sparingly soluble reactant microparticles on the absorption of a gaseous species by a slurry droplet undergoing internal circulation was reported in this paper. The problem studied is relevant to the spray FGD systems. Quasi-steady conservation equations governing mass conservation of the absorbed and reactant species and equations governing the shrinkage of solid particles due to their partial dissolution, were numerically solved using the coordinate system of Kronig and Brink [22].

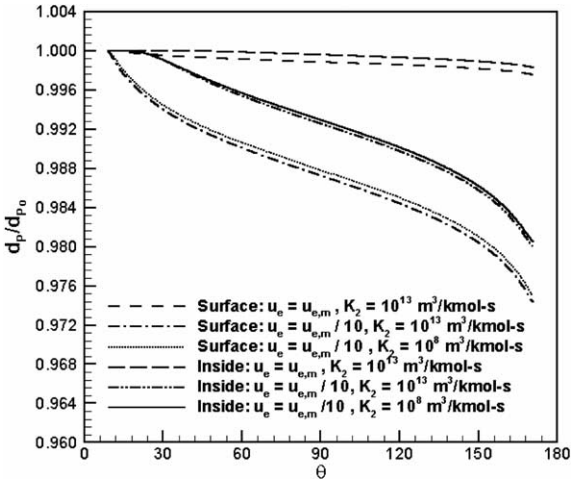

Fig. 7. Some calculated solid particle size variations over a single droplet recirculation. The curves designated as inside represent the streamline with $\xi = 2.69 \times 10^{-3}$.

Calculations were performed for a droplet with unimpeded internal circulation and a droplet for which the internal recirculation was 10 times slower.

The simulation results indicated that a reaction layer (where the absorbed species A is present, namely $X_A > 0$) and a diffusion layer (where the reactant species concentration is affected by the absorption process at droplet surface, namely $X_B < 1$) are formed and developed along the droplet surface. The reactant solid particles enhance the absorption rate by reducing the thickness of the reaction layer and increasing the concentration gradient of the transferred species beneath the droplet surface. Stronger droplet internal circulation reduces the effect of particles due to shorter droplet surface exposure time, however.

Appendix A. Nodalization and numerical solution technique

The computational domain was divided into different segments based on the concentration profiles and different mesh sizes were used in each segment. Along the ξ-direction, two thin strips were defined near the droplet surface (typically defined according to $0 \leqslant \xi < 0.04167$ and $0.04167 \leqslant \xi < 0.1$, respectively), followed by a third region represented by $0.1 \leqslant \xi < \xi_{max}$. Structured meshes were generated with uniform and very fine grids in the two strips near the droplet surface. Typically 450 nodes were used in the first (outermost) layer and 470 nodes were used for the second layer. In the third thick region, where concentration gradients are small, non-uniform and gradually increasing grids toward the droplet interior were generated. Similarly, in the ζ-direction, the northern hemisphere was divided into three zones, with thinnest zone residing near the equator. Non-uniform in (ξ, ζ), but roughly uniform meshes in (η, θ) coordinate system, were generated in each of these regions, such that the equatorial region had the finest grids. The trailing hemisphere was the mirror image of the leading one. The zones were typically defined as follows. The first zone covered $0.95 = \zeta_{0,1} \leqslant \zeta < 0.095$ and had 133 grids. The second zone covered $0.095 \leqslant \zeta < 5.0 \times 10^{-6}$ and had 333 nodes. The third zone covered $5.0 \times 10^{-6} \leqslant \zeta < 0_+$ and included 334 nodes. The singularity associated with the equator ($\zeta = 0$) was avoided by putting the first node point nearest to the equator at a very small distance from the equator (equal to 0.01 times the distance between the next two consecutive nodes). Very good numerical convergence was obtained by using a total of 1000 grids in the ξ-direction and 1600 grids (northern and southern hemispheres collectively) in the ζ-direction.

The central-differencing technique was used and the discretized equations were solved iteratively, using the Line Gauss–Seidel (LGS) method. For a structured grid, the coefficient matrix of the finite-difference equations is banded and special line-by-line iterative techniques such as LGS can be applied. LGS method involves solving the equations representing all the nodes on a sweep line simultaneously. The nodes on $\xi =$ constant lines represented the sweep line for us. The finite-difference equations for each sweep line formed a tri-diagonal matrix and were solved via a standard Tri-Diagonal Matrix Algorithm (TDMA) solver. In the numerical solution, starting from the leading edge of the solution domain and marching along ζ, the equations in the sweep direction (ξ) were simultaneously solved for each $\zeta =$ constant grid line, using values from the previous sweep for the downwind nodes and values from the previous iteration for the upwind nodes, until the trailing edge of the solution domain was reached. The solution over the entire solution domain would then be repeated and continued until convergence was achieved. The criterion for numerical convergence was a maximum change of 5×10^{-7} in the calculated concentrations. For the default case, convergence was achieved with 236 iterations, although for slower recirculation droplets it took more than 1000 iterations.

References

[1] P.A. Ramachandran, M.M. Sharma, Absorption with fast reaction in a slurry containing sparingly soluble fine particles, Chem. Eng. Sci. 24 (1969) 1681–1686.

[2] S. Uchida, K. Koide, M. Shindo, Gas absorption with fast reaction into slurry containing fine particles, Chem. Eng. Sci. 30 (1975) 644–646.

[3] S. Uchida, C.Y. Wen, Rate of gas absorption into a slurry accompanied by instantaneous reaction, Chem. Eng. Sci. 32 (1977) 1277–1281.
[4] S. Uchida, H. Moriguchi, H. Maejima, K. Koide, S. Kageyama, Absorption of sulfur dioxide into limestone slurry in a stirred tank reactor, Can. J. Chem. Eng. 56 (1978) 690–697.
[5] S. Uchida, O. Ariga, Absorption of sulfur dioxide into limestone slurry in a stirred tank, Can. J. Chem. Eng. 63 (1985) 778–783.
[6] E. Sada, H. Kumazawa, M.A. Butt, Chemical absorption into a finite slurry, Chem. Eng. Sci. 34 (1979) 715–718.
[7] E. Sada, H. Kumazawa, Y. Sawada, I. Hashizume, Kinetics of absorption of lean sulfur dioxide into aqueous slurries of calcium carbonate and magnesium sulfate, Chem. Eng. Sci. 36 (1981) 149–155.
[8] E. Sada, Y. Kumazawa, I. Hashizume, M. Kimishima, Desulfurization by limestone slurry with added magnesium sulfate, Chem. Eng. J. 22 (1981) 133–141.
[9] A. Lancia, D. Musmarra, F. Pepe, G. Volpicelli, SO_2 absorption in a bubbling reactor using limestone suspensions, Chem. Eng. Sci. 49 (1994) 4523–4532.
[10] A. Mehra, Gas absorption in reactive slurries: particle dissolution near gas–liquid interface, Chem. Eng. Sci. 51 (1996) 461–477.
[11] A. Muginstein, M. Fichman, C. Gutfinger, Gas absorption in a moving drop containing suspended solids, Int. J. Multiphase Flow 27 (2001) 1079–1094.
[12] S. Uchida, M. Miyachi, O. Ariga, Penetration model of gas absorption into slurry accompanied by an instantaneous irreversible chemical reaction, Can. J. Chem. Eng. 59 (1981) 560–561.
[13] C. Brogren, H.T. Karlsson, Modeling the absorption of SO_2 in a spray scrubber using the penetration theory, Chem. Eng. Sci. 52 (1997) 3085–3099.
[14] W. Pasiuk-Bronikowska, K.J. Rudzinski, Absorption of SO_2 into aqueous system, Chem. Eng. Sci. 46 (1991) 2281–2291.
[15] R. Clift, J.R. Grace, M.E. Weber, Bubbles, Drops and Particles, Academic Press, New York, 1978.
[16] J. Hadamard, Mouvement permanent lent d'une sphere liquid et visqueuse dans un liquid visqueux, Compt. Rend 152 (1911) 1735.
[17] V.G. Levich, Physicochemical Hydrodynamics, Prentice-Hall, New York, 1962.
[18] G.K. Batchelor, On steady laminar flow with closed streamlines at large Reynolds number, J. Fluid Mech. 1 (1956) 177–190.
[19] J.F. Harper, D.W. Moore, The motion of a spherical liquid drop at high Reynolds number, J. Fluid. Mech. 32 (1968) 367–391.
[20] A.S. Brignell, Solute extraction from an internally circulating spherical liquid droplet, Int. J. Heat Mass Transfer 18 (1975) 61–68.
[21] T.H. Chang, J.N. Chung, The effect of surfactants on the motion and transport mechanisms of of condensing droplet in a high Reynolds number flow, AIChE J. 37 (1985) 1149–1156.
[22] R. Kronig, J.C. Brink, On the theory of extraction from falling droplets, Appl. Sci. Res. A 2 (1950) 142–154.
[23] S.M. Ghiaasiaan, D.A. Eghbali, Transient mass transfer of a trace species in an evaporating spherical droplet with internal circulation, Int. J. Heat Mass Transfer 37 (1994) 2287–2295.
[24] I. Bjerle, S. Bengtsson, K. Färnkvist, Absorption of SO_2 in $CaCO_3$ slurry in a laminar jet absorber, Chem. Eng. Sci. 27 (1972) 1853–1861.
[25] M.K. Akbar, S.M. Ghiaasiaan, Modeling the gas absorption in a spray scrubber with dissolving reactive particles, Chem. Eng. Sci., in press.